Realization of Qi-Wu-Zhang model in spin-orbit-coupled ultracold fermions

Ming-Cheng Liang,[1,2,*] Yu-Dong Wei,[1,2,*] Long Zhang ⬤,[1,2,5,*,†] Xu-Jie Wang ⬤,[1,2] Han Zhang,[1,2] Wen-Wei Wang,[1,2]
Wei Qi,[1,2] Xiong-Jun Liu ⬤,[1,2,3,5,‡] and Xibo Zhang ⬤[1,2,4,5,§]

[1]*International Center for Quantum Materials, School of Physics, Peking University, Beijing 100871, China*
[2]*Collaborative Innovation Center of Quantum Matter, Beijing 100871, China*
[3]*International Quantum Academy, Shenzhen 518048, China*
[4]*Beijing Academy of Quantum Information Sciences, Beijing 100193, China*
[5]*Hefei National Laboratory, Hefei 230088, China*

Based on the optical Raman lattice technique, we experimentally realize the Qi-Wu-Zhang model for the quantum anomalous Hall phase in ultracold fermions with two-dimensional (2D) spin-orbit (SO) coupling. We develop an experimental protocol of pump-probe quench measurement to probe, with minimal heating, the resonant spin flipping on a particular quasimomentum subspace called band-inversion surfaces. With this protocol we demonstrate Dirac-type 2D SO coupling in a fermionic system, and detect nontrivial band topology by observing the change of band-inversion surfaces as the two-photon detuning varies. The nontrivial band topology is also observed by slowly loading the atoms into optical Raman lattices and measuring the spin textures. Our results show solid evidence for the realization of the minimal SO-coupled quantum anomalous Hall model, which can provide a feasible platform to investigate novel topological physics including the correlation effects with SO-coupled ultracold fermions.

The quantum anomalous Hall (QAH) effect denotes the quantum Hall effect without the Landau levels due to an external magnetic field [1,2]. Over three decades ago, Haldane proposed the first fundamental model for the QAH effect based on spinless fermions with staggered flux in a honeycomb lattice [3]. However, the QAH phase has been realized and widely studied only in the recent years [4–6] in solid-state experiments based on the considerable progress of topological insulators [7–9], which has been strongly promoted by the other fundamental QAH model proposed by Qi, Wu, and Zhang based on spin-1/2 fermions in a square lattice and two-dimensional (2D) spin-orbit (SO) coupling [10,11].

The Qi-Wu-Zhang model [10] has broad impact on condensed matter research and quantum simulation. First, it is the basic building block of the Bernevig-Hughes-Zhang model [12] underlying the quantum spin Hall effect [7,8,12,13]. Second, it initiated a series of theoretical works [14–17] that inspired the successful experimental realization of the QAH effect based on magnetically doping a topological insulator

[4–6]. Third, unlike the Haldane model where the *s*-wave interaction cannot be directly added, the Qi-Wu-Zhang model allows for incorporating the *s*-wave interaction and thus provides a promising route toward the realization of topological superconductors [7,8,18–20] and topological superfluids [21].

Ultracold atoms provide a highly versatile platform capable of strictly implementing these fundamental QAH models [22]. To realize the Qi-Wu-Zhang model, a novel scheme based on the optical Raman lattice technique was proposed to achieve Dirac-type 2D SO couplings in ultracold fermions [21]. Follow-up studies on 2D SO couplings have been carried out for Bose-Einstein condensates [23–26]. However, the Qi-Wu-Zhang model has yet to be realized in any fermionic system. Such an implementation is related to the noninteracting limit of a four-Fermi-Wilson model [27,28] and will provide a promising platform for further studies of intriguing correlated physics in interacting regimes, including non-Abelian dynamical gauge fields [27,28] and topological superfluidity [21].

Due to their insensitivity to external fields [29], alkaline-earth atoms (AEAs) have additional advantages for realizing highly stable SO-coupled systems and the Qi-Wu-Zhang model. AEAs enable a unique technique, the optical ac Stark shift [30], to achieve stable and spin-dependent ground-state energy shifts [31]. Based on narrow-linewidth transitions, one-dimensional (1D) SO couplings [32–34] have been implemented, where heating due to spontaneous emission is significantly suppressed.

In this Letter, we report an experimental realization of the Qi-Wu-Zhang model in a fermionic system. We implement this model using strontium (^{87}Sr) Fermi gases with 2D SO

---

*These authors contributed equally to this work.

†Current address: School of Physics, Huazhong University of Science and Technology, Wuhan 430074, China.

‡Corresponding author: xiongjunliu@pku.edu.cn

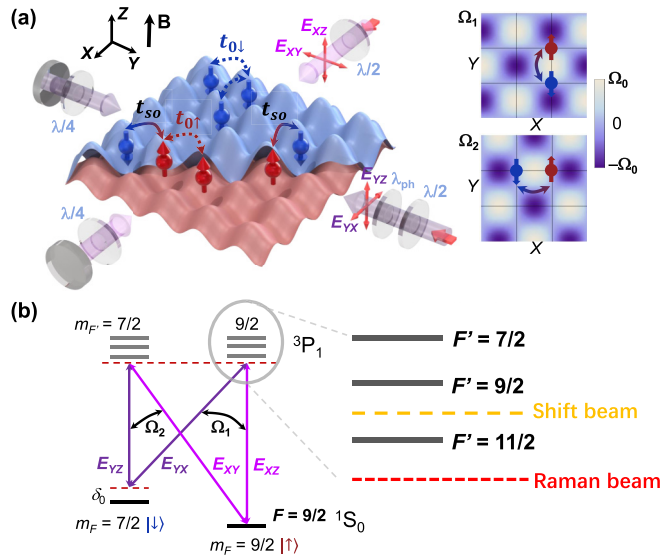§Corresponding author: xibo@pku.edu.cn

FIG. 1. Optical Raman lattice scheme for realizing the Qi-Wu-Zhang model and 2D SO couplings for ultracold fermions. (a) Experimental setup. The magnetic field **B** along the Z direction defines the quantization axis of atoms. Two incident lasers are reflected to construct 2D optical lattices and Raman coupling lattices. The strengths of optical lattices are different for the two spin states (red for $|\uparrow\rangle$ and blue for $|\downarrow\rangle$). Two sets of Raman couplings (Ω_1 and Ω_2) are formed with their maximum values residing in between atomic positions (grid points). (b) Energy level diagram and the Raman coupling scheme. The relative phase $\delta\varphi$ between Ω_1 and Ω_2 is controlled by a composite wave plate $\lambda_{\rm ph}$ shown in (a).

couplings induced by optical Raman lattices. A controlled crossover between 2D and quasi-1D SO couplings and the band topology are observed with a protocol of pump-probe quench measurement developed here, which employs a Raman pulse to drive momentum-dependent spin-flipping. The identification of band topology is further supported by measuring the spin texture in quasimomentum space after slowly loading the fermions into optical Raman lattices. Our work lays an experimental foundation for further studies of topological physics with ultracold fermions.

Experimental setup. We realize the Qi-Wu-Zhang model by implementing an optical Raman lattice scheme [24,25] in ^{87}Sr Fermi gases. As shown in Fig. 1(a), two Raman beams, which are both linearly polarized at a wavelength of $\lambda_0 \approx 689.4$ nm, propagate along the $\hat{X}$ and $-\hat{Y}$ horizontal directions, intersect at the atoms, and are each phase-shifted and retro-reflected to form 2D optical lattices for a pair of spin ground states: $|\uparrow\rangle \equiv\ ^1{\rm S}_0\ |F = \frac{9}{2}, m_F = \frac{9}{2}\rangle$ and $|\downarrow\rangle \equiv |\frac{9}{2}, \frac{7}{2}\rangle$. Two pairs of orthogonal polarization components, (E_{XZ}, E_{YX}) and (E_{XY}, E_{YZ}), form two independent lattices of Raman couplings (Ω_1 and Ω_2) between the $|\uparrow\rangle$ and $|\downarrow\rangle$ states. This 2D optical Raman lattice configuration corresponds to a minimum model of QAH Hamiltonian:

$$\hat{H} = \frac{\mathbf{p}^2}{2m} + V_{\rm latt}(x, y) + \Omega_R(x, y) + \frac{\delta_0}{2}\sigma_z, \quad (1)$$

where m is the atomic mass, $\sigma_{x,y,z}$ are Pauli matrices, and δ_0 is a two-photon Raman detuning. Here, the lattice potential

matrix is given by

$$V_{\rm latt}(x, y) = \begin{pmatrix} V_{{\rm latt}\uparrow}(x, y) & 0 \\ 0 & V_{{\rm latt}\downarrow}(x, y) \end{pmatrix},$$

$$V_{{\rm latt}\uparrow,\downarrow}(x, y) = V_{0X\uparrow,\downarrow} \cos^2 k_0 x + V_{0Y\uparrow,\downarrow} \cos^2 k_0 y, \quad (2)$$

and the Raman coupling matrix

$$\Omega_R(x, y) = \begin{pmatrix} 0 & \Omega_1 + e^{i\delta\varphi}\Omega_2 \\ \Omega_1^* + e^{-i\delta\varphi}\Omega_2^* & 0 \end{pmatrix} \quad (3)$$

shall generate the SO couplings, where $V_{0X\uparrow,\downarrow}$ ($V_{0Y\uparrow,\downarrow}$) denotes the optical lattice depth along the X (Y) direction for the $|\uparrow\rangle$ or $|\downarrow\rangle$ state, $\Omega_1(x, y) = \Omega_{01} \sin k_0 x \cos k_0 y$, $\Omega_2(x, y) = \Omega_{02} \cos k_0 x \sin k_0 y$, $\delta\varphi$ is the relative phase between two sets of Raman couplings, and the lattice spacing and wave vector amplitude are given by $a = \lambda_0/2$ and $k_0 = 2\pi/\lambda_0$, respectively. These Raman beams are detuned relative to the $^1{\rm S}_0(F = \frac{9}{2}) \to\ ^3{\rm P}_1(F' = \frac{11}{2})$ transition by -1 GHz [Fig. 1(b)]. We further define an effective Zeeman splitting as $m_z \equiv \delta_0/2 + (\epsilon_\uparrow - \epsilon_\downarrow)/2$, where $\epsilon_{\uparrow(\downarrow)}$ is the on-site energy of the $|\uparrow\rangle$ ($|\downarrow\rangle$) Wannier function at $\delta_0 = 0$. In the tight-binding regime when only the nearest-neighbor hopping is relevant, Eq. (1) corresponds to the original Qi-Wu-Zhang Hamiltonian [10,23], $\hat{H}(\mathbf{q}) = \sum_{i=x,y,z} h^i(\mathbf{q})\sigma_i + U_0(\mathbf{q})\mathbb{I}$, where $\mathbf{q}$ is the Bloch wave vector, $h^{x/y} = 2t_{\rm so} \sin(q_{y/x}a)$, $h^z = m_z - 2\bar{t}_0[\cos(q_x a) + \cos(q_y a)]$, $U_0(\mathbf{q})$ is an overall energy shift, and $\mathbb{I}$ is the identity matrix. Here, $t_{\rm so}$ and $\bar{t}_0 = (t_{0\uparrow} + t_{0\downarrow})/2$ represent the spin-flip and mean value of spin-conserved ($t_{0\uparrow,\downarrow}$) hopping coefficients, respectively.

To isolate the $|\uparrow\rangle$ and $|\downarrow\rangle$ states from the rest of the ten nuclear spin ground states and to control their energy difference, we apply an additional "shift beam" to induce optical ac Stark shifts for ^{87}Sr atoms [35]. As shown in Fig. 1(b), the shift beam is blue-detuned by 690 MHz from the $F = \frac{9}{2} \to F' = \frac{11}{2}$ transition, which separates out an effective spin-1/2 manifold with an energy difference of about 100 kHz between $|\uparrow\rangle$ and $|\downarrow\rangle$. Based on fractional laser intensity noise controlled to the 10^{-4} level, the stability of ac Stark shift is on the 10-Hz level, which is comparable to the ultrahigh stability in the Zeeman shift of an alkali metal atom under a 10-G magnetic field with 1-ppm control [36].

We prepare and detect SO-coupled fermions as follows. An almost spin-polarized ultracold ^{87}Sr Fermi gas is prepared by optical pumping and subsequent evaporative cooling [35,37]. About 6×10^4 atoms are cooled to a temperature below 200 nK; 85% of these atoms are polarized into the $|\uparrow\rangle$ state. The shift beam intensity is ramped to its final value, and the optical Raman lattices are then turned on suddenly (for quench measurements) or slowly (for slow loading) to generate SO couplings. In the end, we shut off all lasers within 1 μs and perform spin-resolved time-of-flight (TOF) measurements [26,34] to extract the atomic distributions $n_{\uparrow,\downarrow}$ of the $|\uparrow\rangle$ and $|\downarrow\rangle$ states [35]. The spin texture is then given by the spin polarization $P(\mathbf{q}) = \frac{n_\uparrow(\mathbf{q}) - n_\downarrow(\mathbf{q})}{n_\uparrow(\mathbf{q}) + n_\downarrow(\mathbf{q})}$ in the first Brillouin zone.

Pump-probe quench measurement. We develop a protocol of pump-probe quench measurement (PPQM) to probe SO couplings and band topology. As shown in Fig. 2(a), we initially prepare atoms in the $|\uparrow\rangle$ state without lattice, and
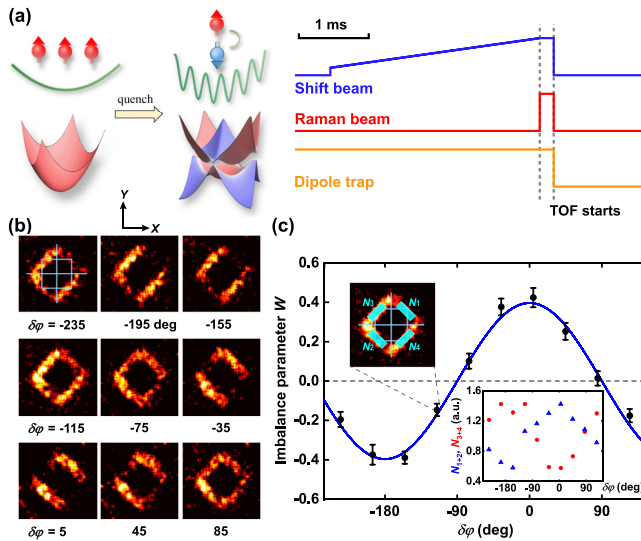
(a)

(b)

(c)

FIG. 2. Pump-probe quench measurement and the demonstration of 2D SO couplings in ultracold fermions. (a) Diagram of the pump-probe quench measurement. (b) TOF images of atoms in the $|\downarrow\rangle$ state under various relative phase $\delta\varphi$ between two Raman couplings. The cyan square marks the size of the first Brillouin zones. (c) Crossover between 2D and quasi-1D SO couplings, presented by the imbalance parameter W as a function of $\delta\varphi$. Black circles are measurements and the blue line is a fit. An optimum 2D SO coupling is achieved at $W = 0$, where the diffracted atomic population in the first and third quadrants (N_{1+2}) equals that in the second and fourth quadrants (N_{3+4}). Upper inset: Illustration of $N_{1,2,3,4}$. Lower inset: Original data of N_{1+2} and N_{3+4}. Error bars represent 1σ statistical uncertainties.

suddenly shine a pulse of optical Raman lattice onto these atoms for a short period of time (denoted as the "pump" part). We then shut off all traps and perform spin-resolved TOF probe of atomic distributions (denoted as the "probe" part), with the results being mapped to the quasimomentum space of the optical Raman lattice. Due to the pulse, atoms in the $|\uparrow\rangle$ state can be selectively pumped to $|\downarrow\rangle$ at those quasimomenta where the lowest spin-up and spin-down bands are inverted and coupled resonantly by two-photon Raman transitions, namely, at the band-inversion surface (BIS) which is a 1D ring or open line structure for the present system in 2D optical Raman lattices [38]. The BISs are an essential concept to depict nontrivial band topology with lower-dimensional information [38–46].

The PPQM technique is a new protocol that combines two important experimental methods: the pump-probe measurement, as widely applied in condensed matter experiments [47–49] and ultrafast optics studies [50,51], and the quench measurement, as applied in previous cold-atom and solid-state experiments [26,44–46,52–59]. Compared with conventional pump-probe measurements, the PPQM protocol pumps atoms from ground state of initial Hamiltonian to the states of a completely new Hamiltonian, rather than to the excited states of the original Hamiltonian, revealing the band topology of the new Hamiltonian. Compared with conventional quench measurements, the PPQM protocol switches on the postquench topological Hamiltonian during the application of a very short pulse ($T_{\text{quench}} = 200\ \mu s$ [35] in this work),

which pumps the atoms to the states of the new Hamiltonian, rather than inducing oscillatory quench dynamics of a steady Hamiltonian. Thus, the PPQM technique can maximally suppress detrimental effects like heating and has the advantage in exploring intriguing topological quantum physics even with only short lifetimes. For example, the PPQM method holds the promise to promote studies of non-Hermitian topological systems [60–64] in the quantum regime, where the characterization of such quantum systems (e.g., those based on ultracold atoms) is often hampered by short lifetime and heating effect.

SO coupling and band topology. We first demonstrate a continuous crossover between 2D and quasi-1D SO couplings based on PPQM. The relative phase $\delta\varphi$ between two Raman couplings (that are proportional to $E_{XZ}E_{YX}^*$ and $E_{XY}E_{YZ}^*$) can be tuned by a variable composite wave plate [35] [see λ_{ph} in Fig. 1(a)] that plays the role of an electro-optic phase modulator controlling the phase shift between E_{YZ} and E_{YX} [25]. Figure 2(b) shows a series of momentum distribution of atoms transferred to $|\downarrow\rangle$, where the typical line segments along the $\hat{X} + \hat{Y}$ and $\hat{X} - \hat{Y}$ directions are consistent with the BIS under the corresponding experimental condition. Four groups of $|\downarrow\rangle$ atoms [marked by N_1 to N_4 in the upper inset of Fig. 2(c)] appear in accordance with the four directions, $(\pm k_0, \pm k_0)$, of SO-coupling-induced momentum transfer. As $\delta\varphi$ changes, N_{1+2} shows an out-of-phase variation with respect to N_{3+4} [lower inset of Fig. 2(c)]. We further define the population imbalance

$$W = \frac{(N_1 + N_2) - (N_3 + N_4)}{(N_1 + N_2) + (N_3 + N_4)}, \tag{4}$$

and observe that W obeys a sinusoidal dependence on $\delta\varphi$ [Fig. 2(c)], as shown by a fit to the function $W = W_{\text{max}} \cos(\delta\varphi)$ [25,35]. Here, $\delta\varphi = 0°$ or $-180°$ corresponds to that only σ_x remains in the Raman coupling matrix, which is similar to 1D SO couplings for fermions in free space [34,65,66]. By contrast, the optimal 2D Dirac-type SO coupling [24] is achieved at $\delta\varphi = \pm 90°$, where balanced $|\downarrow\rangle$ populations of $N_1 \sim N_4$ are observed with $W = 0$. These results reveal the crossover between 2D and quasi-1D SO couplings in our fermionic system, where the optimal 2D SO coupling is chosen as the experimental condition for subsequent measurements.

Next, we perform tomographic studies of the postquench band topology based on PPQM at various two-photon detunings. We choose $V_{0X\uparrow} = V_{0Y\uparrow} = 0.6E_0$, $V_{0X\downarrow} = V_{0Y\downarrow} = 0.3E_0$, $\Omega_{01} = 0.53E_0$, and $\Omega_{02} = 0.22E_0$, where $E_0 = \frac{\hbar^2 k_0^2}{2m}$ is the recoil energy. Figure 3(a) shows that under different m_z values, atoms are pumped to the $|\downarrow\rangle$ state at different quasimomenta in the first Brillouin zone (FBZ), and the maximum density of these $|\downarrow\rangle$ atoms shows ringlike structures in the 2D distributions. As m_z increases from negative to positive, the ring structure shrinks toward the center of FBZ (Γ point), which characterizes a topological transition [38]. Figure 3(b) shows numerical simulations that are very similar to the measurements. We further perform azimuthal averaging of each 2D distribution in Fig. 3(a) and then extract a "ring radius" R_{ring} that corresponds to the maximum density in the 1D profile, as showcased in Figs. 3(c) and 3(d). In Fig. 3(e), the measured ring radii R_{ring} are presented together with a
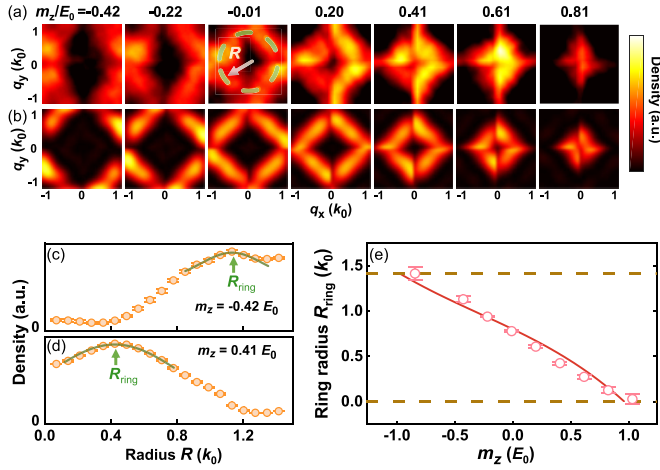
FIG. 3. Tomographic determination of postquench band topology based on PPQM. (a), (b) Experimental observation of band-inversion ring structures (a), represented by pumped $|\downarrow\rangle$ atoms in the first Brillouin zone after quenches, which provides a key feature of the postquench band topology and agrees well with numerical computation (b). The distinct patterns in which band-inversion rings surround the $\Gamma(0, 0)$ or $M(\pm k_0, \pm k_0)$ point mark two different topological regimes. (c), (d) Azimuthally averaged profiles of characteristic 2D distributions in (a), under $m_z/E_0 = -0.42$ (c) and 0.41 (d), which are used to determine the ring radius R_{ring}. (e) Measured radii R_{ring} as a function of m_z are compared with the computed momenta of the BIS (red solid line). Dashed lines mark $R_{ring} = 0$ and $\sqrt{2}k_0$, corresponding to two boundaries of the whole topological regime and an extracted m_z width of $(1.93 \pm 0.12)E_0$ based on the measurements. Error bars represent 1σ statistical uncertainties.

series of computed average radii of the BISs [35], showing good agreement between the measured and computed values. In particular, our measurements cross with the upper and lower boundaries of R_{ring} at two m_z values separated by (9.3 ± 0.6) kHz, corresponding to a width of $(1.93 \pm 0.12)E_0$. This result agrees well with the numerically computed m_z width of $1.93E_0$ for the topological regime based on exact diagonalization of the Hamiltonian Eq. (1) [35] and Chern number analysis [23,35,67], showing the remarkable feature that the PPQM protocol reveals accurate information of the band topology for the Qi-Wu-Zhang model.

Determination of band topology. In order to further reveal the energy band topology, we measure the spin textures after a Fermi gas is slowly loaded into the optical Raman lattices. For this purpose, the Fermi gas is initially populated in the $|\uparrow\rangle$ state and then slowly loaded into 2D optical Raman lattices in 11 ms and further held for 1 ms. This ramp time is an order of magnitude longer than the typical interband relaxation timescales [35] such that our measured spin textures reveal the property of the lowest energy band. Here, the two-photon detuning remains fixed during the loading process; we choose $V_{0X\uparrow} = V_{0Y\uparrow} = 0.7E_0$, $V_{0X\downarrow} = V_{0Y\downarrow} = 1.2E_0$, $\Omega_{01} = 0.80E_0$, and $\Omega_{02} = 0.33E_0$. As shown in Fig. 4(a), the majority of atoms occupy the $|\uparrow\rangle$ state at $m_z = -0.6E_0$, while they occupy the $|\downarrow\rangle$ state at $m_z = 0.6E_0$. The spin texture experiences a smooth change between these two cases as m_z increases. Figure 4(b) shows the corresponding simulations for zero temperature, exhibiting behaviors similar to the mea-
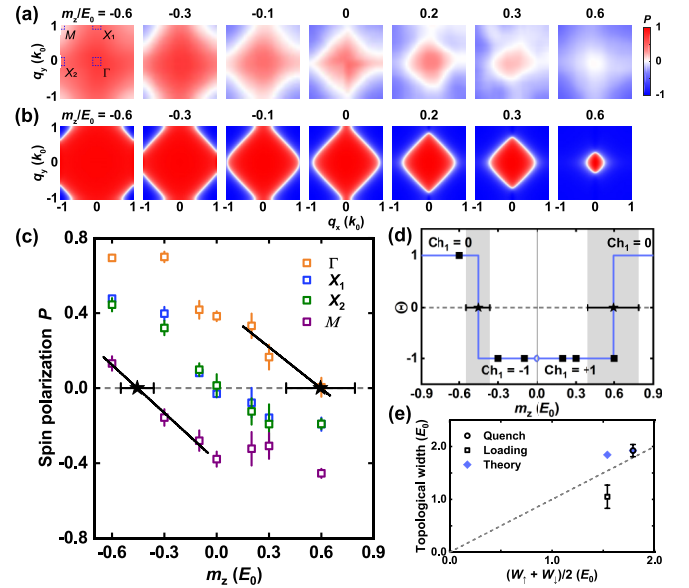

FIG. 4. Determination of band topology based on spin texture measurements. (a) Measured spin textures after slowly loading the atoms into optical Raman lattices. Red and blue colors denote $|\uparrow\rangle$ and $|\downarrow\rangle$, respectively. (b) Numerical simulations for zero temperature. (c) Spin polarizations at four highly symmetric momenta in the FBZ: $\Gamma(0, 0)$, $X_1(0, \pm k_0)$, $X_2(\pm k_0, 0)$, and $M(\pm k_0, \pm k_0)$. (d) The sign product $\Theta = \Pi_{i=1}^{4} \text{sgn}[P(\Lambda_i)]$ and extracted Chern number Ch_1 as a function of m_z. (e) Widths of the topological regime for m_z: PPQM (empty circles), slow loading (empty squares), theory under experimental conditions (solid diamonds), and theory under vanishing SO couplings (dashed line). Here $(W_\uparrow + W_\downarrow)/2$ is the average of the bare ground bandwidths for $|\uparrow\rangle$ and $|\downarrow\rangle$. Error bars represent 1σ statistical uncertainties.

surements [35]. Based on the spin textures, we determine the spin polarizations $P(\Lambda_i)$ at four highly symmetric points $\Lambda_{1,2,3,4} = \Gamma(0, 0)$, $X_1(0, \pm k_0)$, $X_2(\pm k_0, 0)$, and $M(\pm k_0, \pm k_0)$ in the FBZ [Fig. 4(c)], and further determine the Chern number according to the signs of $P(\Lambda_i)$ [23,35,67]. As shown in Fig. 4(d), we extract a trivial-to-topological transition at $m_z/E_0 = (-0.46 \pm 0.09)$, and another topological-to-trivial phase boundary at $m_z/E_0 = (0.60 \pm 0.20)$. These experimentally determined phase boundaries are to be compared with numerically computed results of $m_z/E_0 \approx \pm 0.93$; the measured topological regime has a width that is 57% of the numerical result [Fig. 4(e)]. By comparison, PPQM determines a width of topological regime that is $(100 \pm 6)\%$ of the numerical result. Therefore, both the loading measurement and PPQM reveal the band topologies and are consistent with each other. Furthermore, PPQM is superior in accurately determining the phase boundaries.

Discussion and conclusion. We discuss the lifetime of our system. Near $m_z = 0$, we hold the SO-coupled fermions for different periods of time, measure the decay of the total atom number, and determine a $1/e$ lifetime [35] of $\tau_0 \gtrsim 11$ ms in typical experimental configurations for two-spin 2D-SO-coupled Fermi gases. Even with such limited lifetime, we are able to clearly detect the relevant information on SO couplings and band topology based on the PPQM scheme developed in this work, whereas such important physical

information cannot be detected using conventional quench measurements [35].

At present, τ_0 is limited by technical impediments such as residual moving lattice potentials and has not reached the scattering-rate-limited value [35]. In future experiments, we expect to enhance the lifetime to over 100 ms by implementing a new optical Raman lattice scheme that eliminates moving lattice potentials. With a longer lifetime, the realization of the Qi-Wu-Zhang model in ultracold fermions shall facilitate further studies of equilibrium and nonequilibrium topological physics.

In summary, we have realized the Qi-Wu-Zhang model with 2D-SO-coupled ultracold Fermi gases. We developed a robust pump-probe quench measurement protocol to probe the band topology with minimized heating effect. The band topology with 2D SO coupling is observed by measuring the BISs and spin textures. The realization of the Qi-Wu-Zhang model with spinful ultracold fermions enables the tuning of on-site interactions [68] and can provide a platform for further studies of the interplay between quantum correlations and topological physics [69,70]. Future developments of our system also hold the promise to study correlated quantum dynamics [38,71–73], simulate dynamical gauge fields [27,28,74–78], and ex-plore topological superfluids [19,21,79,80] and topological orders in the interacting regimes [81–83].

X.-J.L. and X.Z. conceived the project. M.-C.L., Y.-D.W., X.-J.W., H.Z., W.-W.W., and W.Q. performed the experiments. L.Z., M.-C.L., and Y.-D.W. performed the numerical computations. All authors contributed to the writing and re-vising of this Letter.

---

[1] K. He, Y. Wang, and Q.-K. Xue, Quantum anomalous Hall effect, Natl. Sci. Rev. **1**, 38 (2014).

[2] C.-X. Liu, S.-C. Zhang, and X.-L. Qi, The quantum anomalous Hall effect: Theory and experiment, Annu. Rev. Condens. Matter Phys. **7**, 301 (2016).

[3] F. D. M. Haldane, Model for a Quantum Hall Effect without Landau Levels: Condensed-Matter Realization of the "Parity Anomaly", Phys. Rev. Lett. **61**, 2015 (1988).

[4] C.-Z. Chang, J. Zhang, X. Feng, J. Shen, Z. Zhang, M. Guo, K. Li, Y. Ou, P. Wei, L.-L. Wang, Z.-Q. Ji, Y. Feng, S. Ji, X. Chen, J. Jia, X. Dai, Z. Fang, S.-C. Zhang, K. He, Y. Wang *et al.*, Experimental observation of the quantum anomalous Hall effect in a magnetic topological insulator, Science **340**, 167 (2013).

[5] J. G. Checkelsky, R. Yoshimi, A. Tsukazaki, K. S. Takahashi, Y. Kozuka, J. Falson, M. Kawasaki, and Y. Tokura, Trajectory of the anomalous Hall effect towards the quantized state in a ferromagnetic topological insulator, Nat. Phys. **10**, 731 (2014).

[6] X. Kou, S.-T. Guo, Y. Fan, L. Pan, M. Lang, Y. Jiang, Q. Shao, T. Nie, K. Murata, J. Tang, Y. Wang, L. He, T.-K. Lee, W.-L. Lee, and K. L. Wang, Scale-Invariant Quantum Anomalous Hall Effect in Magnetic Topological Insulators beyond the Two-Dimensional Limit, Phys. Rev. Lett. **113**, 137201 (2014).

[7] M. Z. Hasan and C. L. Kane, Colloquium: Topological insulators, Rev. Mod. Phys. **82**, 3045 (2010).

[8] X.-L. Qi and S.-C. Zhang, Topological insulators and superconductors, Rev. Mod. Phys. **83**, 1057 (2011).

[9] K. He and Q.-K. Xue, The road to high-temperature quantum anomalous Hall effect in magnetic topological insulators, SPIN **09**, 1940016 (2019).

[10] X.-L. Qi, Y.-S. Wu, and S.-C. Zhang, Topological quantization of the spin Hall effect in two-dimensional paramagnetic semiconductors, Phys. Rev. B **74**, 085308 (2006).

[11] J. K. Asbóth, L. Oroszlány, and A. Pályi, *A Short Course on Topological Insulators* (Springer, Cham, 2016).

[12] B. A. Bernevig, T. L. Hughes, and S.-C. Zhang, Quantum spin Hall effect and topological phase transition in HgTe quantum wells, Science **314**, 1757 (2006).

[13] M. Konig, S. Wiedmann, C. Brune, A. Roth, H. Buhmann, L. W. Molenkamp, X.-L. Qi, and S.-C. Zhang, Quantum spin Hall insulator state in HgTe quantum wells, Science **318**, 766 (2007).

[14] C.-X. Liu, X.-L. Qi, X. Dai, Z. Fang, and S.-C. Zhang, Quantum Anomalous Hall Effect in $Hg_{1-y}Mn_yTe$ Quantum Wells, Phys. Rev. Lett. **101**, 146802 (2008).

[15] X.-L. Qi, T. L. Hughes, and S.-C. Zhang, Topological field theory of time-reversal invariant insulators, Phys. Rev. B **78**, 195424 (2008).

[16] R. Yu, W. Zhang, H.-J. Zhang, S.-C. Zhang, X. Dai, and Z. Fang, Quantized anomalous Hall effect in magnetic topological insulators, Science **329**, 61 (2010).

[17] K. Nomura and N. Nagaosa, Surface-Quantized Anomalous Hall Current and the Magnetoelectric Effect in Magnetically Disordered Topological Insulators, Phys. Rev. Lett. **106**, 166802 (2011).

[18] L. Fu and C. L. Kane, Superconducting Proximity Effect and Majorana Fermions at the Surface of a Topological Insulator, Phys. Rev. Lett. **100**, 096407 (2008).

[19] X.-L. Qi, T. L. Hughes, and S.-C. Zhang, Chiral topological superconductor from the quantum Hall state, Phys. Rev. B **82**, 184516 (2010).

[20] J. Wang, Q. Zhou, B. Lian, and S.-C. Zhang, Chiral topological superconductor and half-integer conductance plateau from quantum anomalous Hall plateau transition, Phys. Rev. B **92**, 064520 (2015).

[21] X.-J. Liu, K. T. Law, and T. K. Ng, Realization of 2D Spin-Orbit Interaction and Exotic Topological Orders in Cold Atoms, Phys. Rev. Lett. **112**, 086401 (2014).

[22] G. Jotzu, M. Messer, R. Desbuquois, M. Lebrat, T. Uehlinger, D. Greif, and T. Esslinger, Experimental realization of the topological Haldane model with ultracold fermions, Nature (London) **515**, 237 (2014).

[23] Z. Wu, L. Zhang, W. Sun, X.-T. Xu, B.-Z. Wang, S.-C. Ji, Y. Deng, S. Chen, X.-J. Liu, and J.-W. Pan, Realization of two-dimensional spin-orbit coupling for Bose-Einstein condensates, Science **354**, 83 (2016).

[24] B.-Z. Wang, Y.-H. Lu, W. Sun, S. Chen, Y. Deng, and X.-J. Liu, Dirac-, Rashba-, and Weyl-type spin-orbit couplings: Toward experimental realization in ultracold atoms, Phys. Rev. A **97**, 011605(R) (2018).

[25] W. Sun, B.-Z. Wang, X.-T. Xu, C.-R. Yi, L. Zhang, Z. Wu, Y. Deng, X.-J. Liu, S. Chen, and J.-W. Pan, Highly Controllable and Robust 2D Spin-Orbit Coupling for Quantum Gases, Phys. Rev. Lett. **121**, 150401 (2018).

[26] W. Sun, C.-R. Yi, B.-Z. Wang, W.-W. Zhang, B. C. Sanders, X.-T. Xu, Z.-Y. Wang, J. Schmiedmayer, Y. Deng, X.-J. Liu, S. Chen, and J.-W. Pan, Uncover Topology by Quantum Quench Dynamics, Phys. Rev. Lett. **121**, 250403 (2018).

[27] L. Ziegler, E. Tirrito, M. Lewenstein, S. Hands, and A. Bermudez, Correlated Chern insulators in two-dimensional Raman lattices: A cold-atom regularization of strongly-coupled four-Fermi field theories, Phys. Rev. Res. **4**, L042012 (2022).

[28] L. Ziegler, E. Tirrito, M. Lewenstein, S. Hands, and A. Bermudez, Large-*N* Chern insulators: Lattice field theory and quantum simulation approaches to correlation effects in the quantum anomalous Hall effect, Ann. Phys. **439**, 168763 (2022).

[29] A. J. Daley, Quantum computing and quantum simulation with group-II atoms, Quantum Inf. Process. **10**, 865 (2011).

[30] G. W. F. Drake (Ed.), *Atomic, Molecular, and Optical Physics Handbook* (American Institute of Physics, Woodbury, NY, 1996).

[31] J. Ye, H. J. Kimble, and H. Katori, Quantum state engineering and precision metrology using state-insensitive light traps, Science **320**, 1734 (2008).

[32] L. F. Livi, G. Cappellini, M. Diem, L. Franchi, C. Clivati, M. Frittelli, F. Levi, D. Calonico, J. Catani, M. Inguscio, and L. Fallani, Synthetic Dimensions and Spin-Orbit Coupling with an Optical Clock Transition, Phys. Rev. Lett. **117**, 220401 (2016).

[33] S. Kolkowitz, S. L. Bromley, T. Bothwell, M. L. Wall, G. E. Marti, A. P. Koller, X. Zhang, A. M. Rey, and J. Ye, Spin-orbit-coupled fermions in an optical lattice clock, Nature (London) **542**, 66 (2017).

[34] B. Song, C. He, S. Zhang, E. Hajiyev, W. Huang, X.-J. Liu, and G.-B. Jo, Spin-orbit-coupled two-electron Fermi gases of ytterbium atoms, Phys. Rev. A **94**, 061604(R) (2016).

[35] See Supplemental Material at http://link.aps.org/supplemental/10.1103/PhysRevResearch.5.L012006 for details on (I) experimental techniques in preparing and detecting the Fermi gases, (II) demonstration on coherence between two sets of Raman couplings, (III) crossover between 2D and quasi-1D SO couplings, (IV) more information on pump-probe quench measurement, (V) theoretical and experimental as-

pects in determining the band topology, (VI) lifetime of 2D-SO-coupled Fermi gas. The Supplemental Material cites Refs. [23–26,34,45,65–67,84].

[36] X.-T. Xu, Z.-Y. Wang, R.-H. Jiao, C.-R. Yi, W. Sun, and S. Chen, Ultra-low noise magnetic field for quantum gases, Rev. Sci. Instrum. **90**, 054708 (2019).

[37] W. Qi, M.-C. Liang, H. Zhang, Y.-D. Wei, W.-W. Wang, X.-J. Wang, and X. Zhang, Experimental realization of degenerate Fermi gases of ^{87}Sr atoms with 10 or two spin components, Chin. Phys. Lett. **36**, 093701 (2019).

[38] L. Zhang, L. Zhang, S. Niu, and X.-J. Liu, Dynamical classification of topological quantum phases, Sci. Bull. **63**, 1385 (2018).

[39] H. Hu and E. Zhao, Topological Invariants for Quantum Quench Dynamics from Unitary Evolution, Phys. Rev. Lett. **124**, 160402 (2020).

[40] B. Zhu, Y. Ke, H. Zhong, and C. Lee, Dynamic winding number for exploring band topology, Phys. Rev. Res. **2**, 023043 (2020).

[41] J. Ye and F. Li, Emergent topology under slow nonadiabatic quantum dynamics, Phys. Rev. A **102**, 042209 (2020).

[42] X.-L. Yu, W. Ji, L. Zhang, Y. Wang, J. Wu, and X.-J. Liu, Quantum dynamical characterization and simulation of topological phases with high-order band inversion surfaces, PRX Quantum **2**, 020320 (2021).

[43] L. Li, W. Zhu, and J. Gong, Direct dynamical characterization of higher-order topological phases with nested band inversion surfaces, Sci. Bull. **66**, 1502 (2021).

[44] B. Song, C. He, S. Niu, L. Zhang, Z. Ren, X.-J. Liu, and G.-B. Jo, Observation of nodal-line semimetal with ultracold fermions in an optical lattice, Nat. Phys. **15**, 911 (2019).

[45] C.-R. Yi, L. Zhang, L. Zhang, R.-H. Jiao, X.-C. Cheng, Z.-Y. Wang, X.-T. Xu, W. Sun, X.-J. Liu, S. Chen, and J.-W. Pan, Observing Topological Charges and Dynamical Bulk-Surface Correspondence with Ultracold Atoms, Phys. Rev. Lett. **123**, 190603 (2019).

[46] Y. Wang, W. Ji, Z. Chai, Y. Guo, M. Wang, X. Ye, P. Yu, L. Zhang, X. Qin, P. Wang, F. Shi, X. Rong, D. Lu, X.-J. Liu, and J. Du, Experimental observation of dynamical bulk-surface correspondence in momentum space for topological phases, Phys. Rev. A **100**, 052328 (2019).

[47] J. Lloyd-Hughes, P. M. Oppeneer, T. P. dos Santos, A. Schleife, S. Meng, M. A. Sentef, M. Ruggenthaler, A. Rubio, I. Radu, M. Murnane, X. Shi, H. Kapteyn, B. Stadtmuller, K. M. Dani, F. H. da Jornada, E. Prinz, M. Aeschlimann, R. L. Milot, M. Burdanova, J. Boland *et al.*, The 2021 ultrafast spectroscopic probes of condensed matter roadmap, J. Phys.: Condens. Matter **33**, 353001 (2021).

[48] A. L. Cavalieri, N. Muller, T. Uphues, V. S. Yakovlev, A. Baltuska, B. Horvath, B. Schmidt, L. Blumel, R. Holzwarth, S. Hendel, M. Drescher, U. Kleineberg, P. M. Echenique, R. Kienberger, F. Krausz, and U. Heinzmann, Attosecond spectroscopy in condensed matter, Nature (London) **449**, 1029 (2007).

[49] J. Yang, R. Dettori, J. P. F. Nunes, N. H. List, E. Biasin, M. Centurion, Z. Chen, A. A. Cordones, D. P. Deponte, T. F. Heinz, M. E. Kozina, K. Ledbetter, M.-F. Lin, A. M. Linderberg, M. Mo, A. Nilsson, X. Shen, T. J. A. Wolf, D. Donadio, K. J. Gaffney *et al.*, Direct observation of ultrafast hydrogen bond strengthening in liquid water, Nature (London) **596**, 531 (2021).

[50] M. Maiuri, M. Garavelli, and G. Cerullo, Ultrafast spectroscopy: State of the art and open challenges, J. Am. Chem. Soc. **142**, 3 (2020).

[51] A. H. Zewail, Femtochemistry: Atomic-scale dynamics of the chemical bond using ultrafast lasers, Angew. Chem. Int. Ed. **39**, 2586 (2000).

[52] M. Greiner, O. Mandel, T. W. Hansch, and I. Bloch, Collapse and revival of the matter wave field of a Bose-Einstein condensate, Nature (London) **419**, 51 (2002).

[53] M. Mancini, G. Pagano, G. Cappellini, L. Livi, M. Rider, J. Catani, C. Sias, P. Zoller, M. Inguscio, M. Dalmonte, and L. Fallani, Observation of chiral edge states with neutral fermions in synthetic Hall ribbons, Science **349**, 1510 (2015).

[54] B. K. Stuhl, H.-I. Lu, L. M. Aycock, D. Genkina, and I. B. Spielman, Visualizing edge states with an atomic Bose gas in the quantum Hall regime, Science **349**, 1514 (2015).

[55] N. Fläschner, B. S. Rem, M. Tarnowski, D. Vogel, D.-S. Luhmann, K. Sengstock, and C. Weitenberg, Experimental reconstruction of the Berry curvature in a Floquet Bloch band, Science **352**, 1091 (2016).

[56] M. Tarnowski, F. N. Unal, N. Flaschner, B. S. Rem, A. Eckardt, K. Sengstock, and C. Weitenberg, Measuring topology from dynamics by obtaining the Chern number from a linking number, Nat. Commun. **10**, 1728 (2019).

[57] W. Ji, L. Zhang, M. Wang, L. Zhang, Y. Guo, Z. Chai, X. Rong, F. Shi, X.-J. Liu, Y. Wang, and J. Du, Quantum Simulation for Three-Dimensional Chiral Topological Insulator, Phys. Rev. Lett. **125**, 020504 (2020).

[58] B. Chen, S. Li, X. Hou, F. Ge, F. Zhou, P. Qian, F. Mei, S. Jia, N. Xu, and H. Shen, Digital quantum simulation of Floquet topological phases with a solid-state quantum simulator, Photonics Res. **9**, 81 (2021).

[59] J. Niu, T. Yan, Y. Zhou, Z. Tao, X. Li, W. Liu, L. Zhang, H. Jia, S. Liu, Z. Yan, Y. Chen, and D. Yu, Simulation of higher-order topological phases and related topological phase transitions in a superconducting qubit, Sci. Bull. **66**, 1168 (2021).

[60] E. J. Bergholtz, J. C. Budich, and F. K. Kunst, Exceptional topology of non-Hermitian systems, Rev. Mod. Phys. **93**, 015005 (2021).

[61] J. M. Zeuner, M. C. Rechtsman, Y. Plotnik, Y. Lumer, S. Nolte, M. S. Rudner, M. Segev, and A. Szameit, Observation of a Topological Transition in the Bulk of a Non-Hermitian System, Phys. Rev. Lett. **115**, 040402 (2015).

[62] H. Zhou, C. Peng, Y. Yoon, C. W. Hsu, K. A. Nelson, L. Fu, J. D. Joannopoulos, M. Soljacic, and B. Zhen, Observation of bulk Fermi arc and polarization half charge from paired exceptional points, Science **359**, 1009 (2018).

[63] T. Helbig, T. Hofmann, S. Imhof, M. Abdelghany, T. Kiessling, L. W. Molenkamp, C. H. Lee, A. Szameit, M. Greiter, and R. Thomale, Generalized bulk-boundary correspondence in non-Hermitian topolectrical circuits, Nat. Phys. **16**, 747 (2020).

[64] A. Ghatak, M. Brandenbourger, J. v. Wezel, and C. Coulais, Observation of non-Hermitian topology and its bulk-edge correspondence in an active mechanical metamaterial, Proc. Nat. Acad. Sci. **117**, 29561 (2020).

[65] P. Wang, Z.-Q. Yu, Z. Fu, J. Miao, L. Huang, S. Chai, H. Zhai, and J. Zhang, Spin-Orbit Coupled Degenerate Fermi Gases, Phys. Rev. Lett. **109**, 095301 (2012).

[66] L. W. Cheuk, A. T. Sommer, Z. Hadzibabic, T. Yefsah, W. S. Bakr, and M. W. Zwierlein, Spin-Injection Spectroscopy of a Spin-Orbit Coupled Fermi Gas, Phys. Rev. Lett. **109**, 095302 (2012).

[67] X.-J. Liu, K. T. Law, T. K. Ng, and P. A. Lee, Detecting Topological Phases in Cold Atoms, Phys. Rev. Lett. **111**, 120402 (2013).

[68] R. Zhang, Y. Cheng, P. Zhang, and H. Zhai, Controlling the interaction of ultracold alkaline-earth atoms, Nat. Rev. Phys. **2**, 213 (2020).

[69] M. Hohenadler and F. F. Assaad, Correlation effects in two-dimensional topological insulators, J. Phys.: Condens. Matter **25**, 143201 (2013).

[70] S. Rachel, Interacting topological insulators: A review, Rep. Prog. Phys. **81**, 116501 (2018).

[71] M. McGinley and N. R. Cooper, Interacting symmetry-protected topological phases out of equilibrium, Phys. Rev. Res. **1**, 033204 (2019).

[72] L. Pastori, S. Barbarino, and J. C. Budich, Signatures of topology in quantum quench dynamics and their interrelation, Phys. Rev. Res. **2**, 033259 (2020).

[73] L. Zhang, L. Zhang, Y. Hu, S. Niu, and X.-J. Liu, Nonequilibrium characterization of equilibrium correlated quantum phases, Phys. Rev. B **103**, 224308 (2021).

[74] J. Dalibard, F. Gerbier, G. Juzeliūnas, and P. Öhberg, Colloquium: Artificial gauge potentials for neutral atoms, Rev. Mod. Phys. **83**, 1523 (2011).

[75] N. Goldman, G. Juzeliūnas, P. Öhberg, and I. B. Spielman, Light-induced gauge fields for ultracold atoms, Rep. Prog. Phys. **77**, 126401 (2014).

[76] U.-J. Wiese, Ultracold quantum gases and lattice systems: Quantum simulation of lattice gauge theories, Ann. Phys. **525**, 777 (2013).

[77] E. Zohar, J. I. Cirac, and B. Reznik, Quantum simulations of lattice gauge theories using ultracold atoms in optical lattices, Rep. Prog. Phys. **79**, 014401 (2016).

[78] M. Aidelsburger, L. Barbiero, A. Bermudez, T. Chanda, A. Dauphin, D. Gonzalez-Cuadra, P. R. Grzybowski, S. Hands, F. Jendrzejewski, J. Junemann, G. Juzeliūnas, V. Kasper, A. Piga, S.-J. Ran, M. Rizzi, G. Sierra, L. Tagliacozzo, E. Tirrito, T. V. Zache, J. Zakrzewski *et al.*, Cold atoms meet lattice gauge theory, Philos. Trans. R. Soc. A **380**, 20210064 (2021).

[79] C. Zhang, S. Tewari, R. M. Lutchyn, and S. Das Sarma, $p_x + ip_y$ Superfluid from s-Wave Interactions of Fermionic Cold Atoms, Phys. Rev. Lett. **101**, 160401 (2008).

[80] M. Sato, Y. Takahashi, and S. Fujimoto, Non-Abelian Topological Order in s-Wave Superfluids of Ultracold Fermionic Atoms, Phys. Rev. Lett. **103**, 020401 (2009).

[81] X.-J. Liu, Z.-X. Liu, K. T. Law, W. V. Liu, and T. K. Ng, Chiral topological orders in an optical Raman lattice, New J. Phys. **18**, 035004 (2016).

[82] J. Radić, A. Di Ciolo, K. Sun, and V. Galitski, Exotic Quantum Spin Models in Spin-Orbit-Coupled Mott Insulators, Phys. Rev. Lett. **109**, 085303 (2012).

[83] W. S. Cole, S. Zhang, A. Paramekanti, and N. Trivedi, Bose-Hubbard Models with Synthetic Spin-Orbit Coupling: Mott Insulators, Spin Textures, and Superfluidity, Phys. Rev. Lett. **109**, 085302 (2012).

[84] J. H. Denschlag, J. E. Simsarian, H. Haffner, C. McKenzie, A. Browaeys, D. Cho, K. Helmerson, S. L. Rolston, and W. D. Phillips, A Bose-Einstein condensate in an optical lattice, J. Phys. B: At. Mol. Opt. Phys. **35**, 3095 (2002).